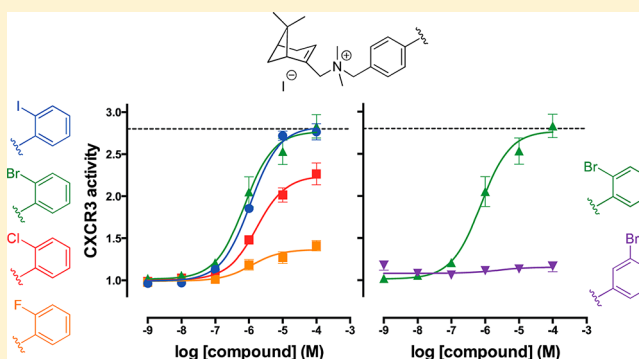


Chemical Subtleties in Small-Molecule Modulation of Peptide Receptor Function: The Case of CXCR3 Biaryl-Type Ligands

Maikel Wijtmans,^{†,§} Danny J. Scholten,^{†,§} Luc Roumen,^{†,§} Meritxell Canals,^{†,||} Hans Custers,[†] Marjolein Glas,[†] Marlies C. A. Vreeker,[†] Frans J. J. de Kanter,[‡] Chris de Graaf,[†] Martine J. Smit,[†] Iwan J. P. de Esch,[†] and Rob Leurs^{*,†}[†]Leiden/Amsterdam Center for Drug Research, Division of Medicinal Chemistry, Faculty of Sciences, VU University Amsterdam, The Netherlands[‡]Division of Organic and Inorganic Chemistry, Faculty of Sciences, VU University Amsterdam, The Netherlands

S Supporting Information

ABSTRACT: The G protein-coupled chemokine receptor CXCR3 plays a role in numerous inflammatory events. The endogenous ligands for the chemokine receptors are peptides, but in this study we disclose small-molecule ligands that are able to activate CXCR3. A class of biaryl-type compounds that is assembled by convenient synthetic routes is described as a new class of CXCR3 agonists. Intriguingly, structure–activity relationship and structure–function relationship studies reveal that subtle chemical modifications on the outer aryl ring (e.g., either the size or position of a halogen atom) result in a full spectrum of agonist efficacies on CXCR3. Quantum mechanics calculations and nuclear Overhauser effect spectroscopy NMR studies suggest that the biaryl dihedral angle and the electronic nature of *ortho*-substituents play an important role in determining agonist efficacies. Compounds **38** (VUF11222) and **39** (VUF11418) are the first reported nonpeptidomimetic agonists on CXCR3, rendering them highly useful chemical tools for detailed assessment of CXCR3 activation as well as for studying downstream CXCR3 signaling.



1. INTRODUCTION

G protein-coupled receptors (GPCRs) form one of the therapeutically most relevant protein families, and around one-third of the available small-molecule drugs target GPCRs.¹ Despite this therapeutic importance, it is often still unclear which structural determinants of the small molecules underlie the functional outcome of ligand–GPCR binding. This question is perhaps most intriguing in the case of peptide GPCRs, which signal as a result of the binding of large peptides.

A well-known class of peptide GPCRs are the chemokine receptors, 19 subtypes of which are currently known.² Chemokine receptors are activated by chemokines, which are chemotactic cytokine peptides that control leukocyte homeostasis, as well as leukocyte recruitment to sites of inflammation or infection. As such, the chemokine system is a key player in the human immune system.³ The chemokine receptor CXCR3 is expressed on various immune cells, including T-cells, and recognizes three endogenous agonist ligands, CXCL9 (11.7 kDa), CXCL10 (8.6 kDa), and CXCL11 (8.3 kDa). Upregulation of CXCR3 and its ligands is linked to a variety of immune-related disorders. The notion of CXCR3 as an interesting therapeutic target is reflected in the high number of reports^{4–6} describing the discovery and optimization of small-molecule CXCR3 antagonists from many different chemotypes,

one example being the frequently used antagonist **1** (NBI-74330).⁷ Small-molecule agonism of CXCR3 has been studied less widely, likely because evidence for the therapeutic value of CXCR3 agonism is scarce and relatively preliminary.^{8,9} Another explanation for this apparent deficiency might be that it is easier to inhibit peptide receptor activation by small molecules than to mimic the specific action of the endogenous peptide agonist. Only one paper disclosing small-molecule agonists of CXCR3 has appeared, reporting on two agonist chemotypes which both clearly bear peptidomimetic character (**2a,b** and **3**, Figure 1).¹⁰ In fact, structure–activity relationship (SAR) studies have revealed that the basic amino acid side chain is crucial in activating CXCR3,¹⁰ and conformational calculations on **2b** have shown that this compound probably mimics the “30s loop” of CXCL10 which includes Arg38.¹¹ Several of these peptidomimetics have since been pharmacologically studied *in vitro* and *in vivo*.^{8,12,13} Even though several X-ray structures for the related chemokine receptor CXCR4 have been elucidated recently,¹⁴ ligand-based information such as the SAR and structure–function relationship (SFR) is still crucial to provide insights into molecular determinants of ligand-induced (chemo-

Received: August 28, 2012

Published: November 14, 2012

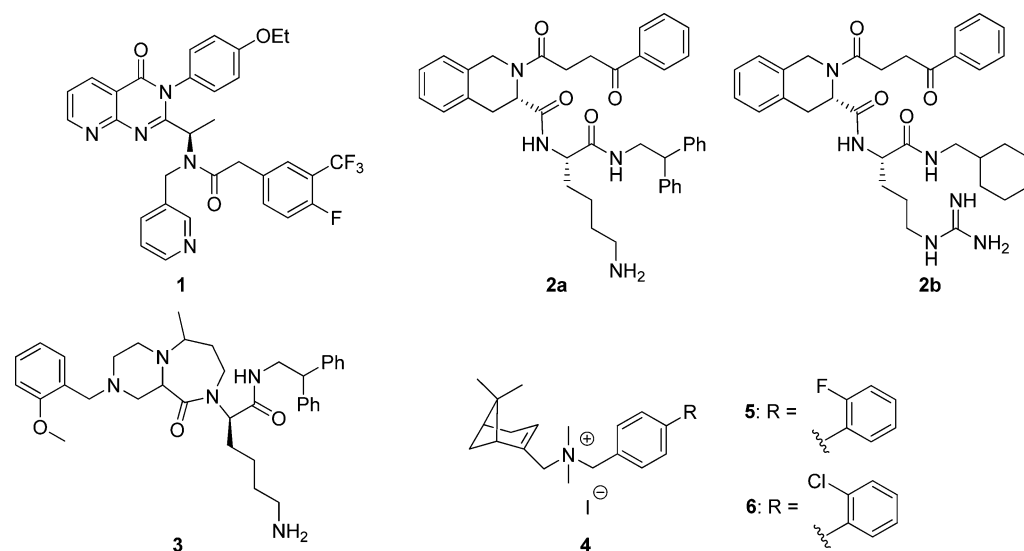
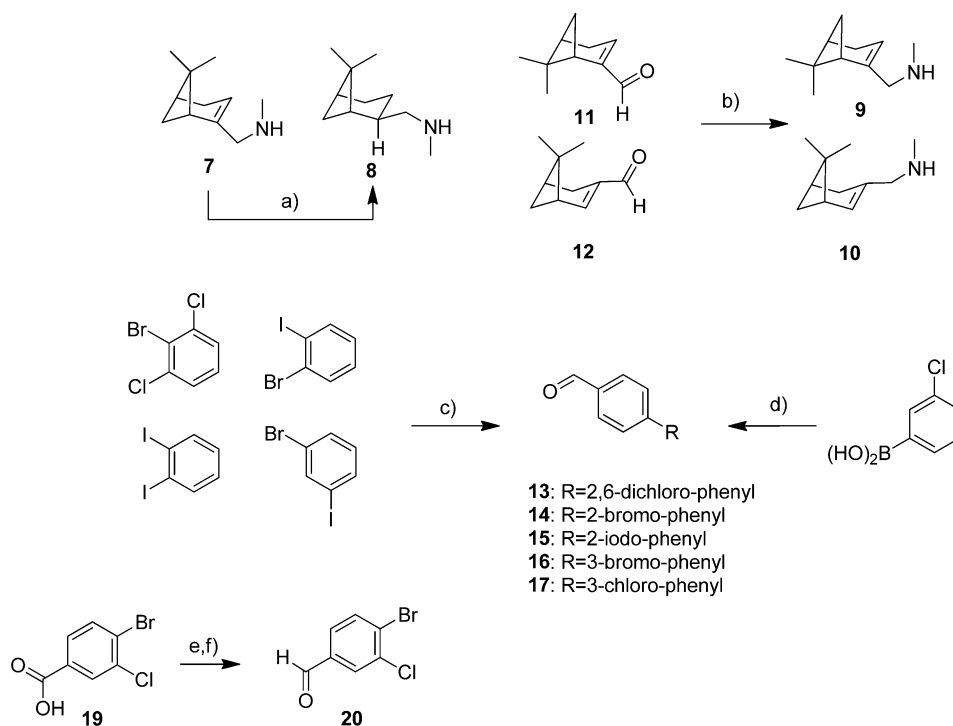


Figure 1. Chemical structures of selected CXCR3 ligands.

Scheme 1. Synthesis of Building Blocks^a

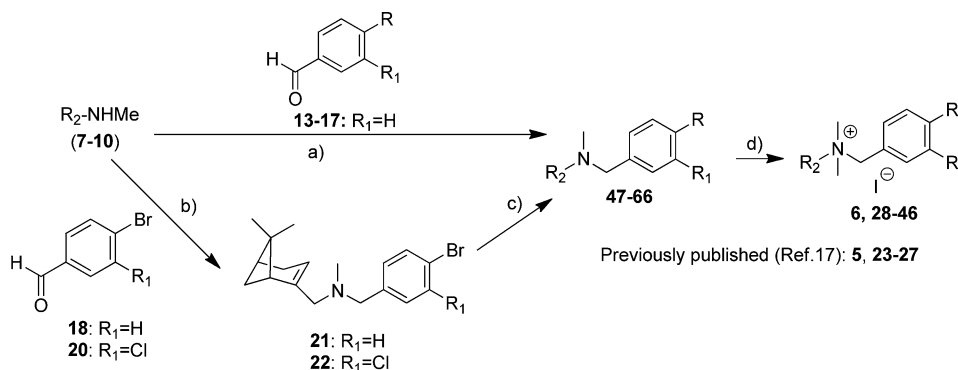


^aReagents and conditions: (a) H_2 , Pd/C, MeOH, 23 h, rt, 72%; (b) (1) H_2NMe , MeOH/EtOH, 1–20 h, rt; (2) NaBH_4 , 2 h, rt, **9**: 50%, **10**: 14% as HCl salt; (c) $\text{Pd}(\text{PPh}_3)_4$, 4- $\text{CHOPh}(\text{OH})_2$, Na_2CO_3 , DME, H_2O , 60–90 min, microwave, 56–91%; (d) $\text{Pd}(\text{PPh}_3)_4$, 4-BrPhCHO (**18**), Na_2CO_3 , DME, H_2O , 7 h, reflux, 85%; (e) $\text{BH}_3 \cdot \text{THF}$, THF, 2.5 h, rt; (f) MnO_2 , DCM, 5 d, rt, 65% from **19**.

kine) GPCR modulation.^{15,16} As such, studies aimed at unraveling ligand-mediated CXCR3 activation and its cellular consequences would greatly benefit from studies on non-peptidomimetic small-molecule activators of CXCR3.

We have recently reported on biaryl-type CXCR3 ligands (**4**, Figure 1), obtained after several rounds of modification following a medium-throughput screen performed in our laboratories.¹⁷ The SAR of scaffold **4** showed varying effects in affinity upon modulation of the “outer” aryl group R. Key members of this chemotype were found to behave as antagonists.¹⁷ In the current paper, we describe how these

compounds can be turned into CXCR3 (full) agonists using intriguingly subtle activation triggers such as manipulation of the size of a halogen substituent as well as of the halogen position. These compounds display the full spectrum of functional efficacies in CXCR3 activation and include the first reported nonpeptidomimetic full agonists on CXCR3. We present pharmacological, nuclear Overhauser effect spectroscopy NMR (NOESY NMR), and quantum mechanics (QM) studies to identify the molecular features that are responsible for the specific functional activity.

Scheme 2. Synthesis of Final Compounds^a

^aReagents and conditions: (a) NaBH(OAc)₃, DCE, rt, 4 h to 2 d, 43–92%; (b) NaBH(OAc)₃, DCE, rt, 20 h, 21: 71% as HCl salt, 22: 78%; (c) Pd(PPh₃)₄, RB(OH)₂, Na₂CO₃, H₂O, DME or *i*PrOH/toluene, microwave, 60–90 min, 34–92%; (d) DCM, MeI, 1–5 d, rt, 22–88%.

2. RESULTS AND DISCUSSION

2.1. Synthesis. All final salts **6** and **28–46** were prepared as outlined in Schemes 1 and 2. The syntheses of analogues **5** and **23–27** through similar routes have been reported by us previously.¹⁷ Hydrogenation of key amine building block **7**¹⁷ provided **8**, with 2D NMR spectroscopy indicating an *endo* geometry. Stereoisomeric analogue **9** and regioisomeric analogue **10** were prepared from the corresponding aldehydes **11** and **12**.^{18,19} Biaryl aldehydes **13–17** were prepared through a Suzuki reaction of an appropriate boronic acid and a complementary halogenated precursor. This “reversed” pre-assembly²⁰ of the biaryl moiety in **13–17** was initially pursued because we observed that 2-bromophenylboronic acid and 2,6-dichlorophenylboronic acid proved difficult to couple to **21** in the alternative Suzuki strategy depicted in Scheme 2. Thereafter, the former procedure was also applied to several other substrates. Substantial amounts of disubstituted product were obtained in the formation of **15** despite the 5-fold excess of 1,2-diiodobenzene. Chlorine-containing building block **20** was prepared through a reduction of the corresponding carboxylic acid **19** to the alcohol followed by an oxidation.

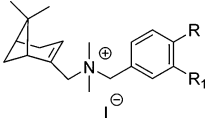
The syntheses of all final compounds (Scheme 2) proceeded mostly along the general routes previously published.¹⁷ Thus, tertiary amine precursors **47–66** were obtained through two approaches. One approach uses a reductive amination to connect a preassembled biarylaldehyde (**13–17**) to building blocks **7–10**. The other approach is a two-step process, starting with reductive alkylation of **7** using aldehyde **18** or **20** to give bromides **21** and **22**, respectively. This was followed by a microwave Suzuki reaction of **21** and **22** and an appropriate boronic acid. Tertiary amine precursors **47–66** were then methylated with MeI to the final ammonium salts **6** and **28–46** in moderate to excellent yield.

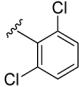
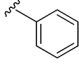
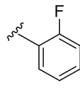
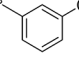
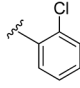
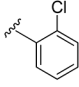
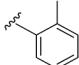
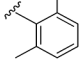
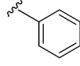
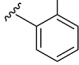
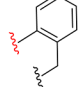
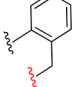
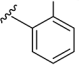
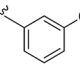
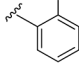
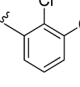
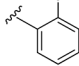
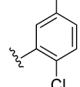
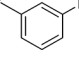
2.2. Structure–Function Relationships. In the SAR efforts on scaffold **4**, the difference in affinity between *o*-F compound **5** and its *meta*-analogue had previously indicated *meta*-substitution of the outer phenyl ring as a means to achieve affinity.¹⁷ More recently, we prepared and tested the *o*-Cl derivative **6**. Interestingly, when subjected to our previously used¹⁷ functional CXCR3 assay recording [³H]-inositolphosphate accumulation after stimulation with CXCL10, **6** did not show any inhibition of CXCL10 responses despite full receptor occupancy (not shown), suggesting that **6** may possess residual agonist activity. Indeed, in a [³⁵S]GTPγS (guanosine 5′-*O*-[γ-thio]triphosphate) functional assay, in

which the native coupling of CXCR3 to G proteins is left intact, **6** proved to be a partial agonist ($\alpha = 0.73$) with micromolar potency (pEC₅₀ = 5.8) (Table 1, Figure 2). This partial agonist activity could be abolished by addition of CXCR3-selective antagonist **17** (Figure S1A, Supporting Information) and by our previously reported antagonist **27** (VUF10990)¹⁷ (data not shown). Moreover, no functional response for **6** was detected in cell membranes that did not express CXCR3 (Figure S1C), suggesting that the observed functional effect for **6** was a consequence of CXCR3 receptor activation. These interesting findings on a nonpeptidomimetic scaffold, which is readily assembled through straightforward synthesis, inspired us to an in-depth investigation of the molecular determinants for activation of the CXCR3 receptor by this ammonium salt scaffold. The corresponding tertiary amines were not investigated because their affinities are expected to be considerably lower compared to those of the ammonium salts, as generally observed in this class.¹⁷

2.2.1. Exploration of Biaryl Substitution. The newly synthesized ammonium salts bind to CXCR3 with affinities ranging from pK_i = 5.7 to pK_i = 7.3 in a radioligand binding displacement assay ([¹²⁵I]CXCL10). Figure 2A shows representative binding curves. All compounds were also analyzed in the [³⁵S]GTPγS functional assay to investigate potency (pEC₅₀) and efficacy (α) at CXCR3 (Table 1). Concentration ranges in the [³⁵S]GTPγS functional assay were chosen such that sufficient receptor occupancy was ensured. The profile of **6** was compared to those of a small set of ammonium salts previously reported by us (**23–27**).¹⁷ Compounds **23** and **24** (lacking the biaryl moiety) as well as **25** and **26** (having an undecorated (un)constrained biaryl system) showed little to no agonistic response ($\alpha \leq 0.1$). Remarkably, a shift of the Cl atom in **6** to the *meta*-position (giving **27**) abolished the agonistic activity. These findings indicate the *ortho*-position on the outer phenyl ring of the biaryl system to be important for receptor activation. With the Cl atom being maintained at this position, the effect of an additional Cl substituent was explored (**28–30**). This yielded partial agonists, which are all weaker than compound **6** with α values ranging from 0.31 to 0.64 (Table 1). Recognizing hindered rotation around the biaryl axis as a potential key factor for CXCR3 agonism, three compounds with a Cl atom on the *ortho*-position of the inner ring were also investigated (**31–33**). However, only **33** showed substantial agonism ($\alpha = 0.30$) (Table 1), arguably because it contains an *o*-Cl moiety on the

Table 1. General Scan of Substituents on the Outer and Inner Phenyl Rings



#	R	R ₁	Affinity (pK _i) ^a	Potency (pEC ₅₀) ^b	Efficacy (α) ^{b,c}	#	R	R ₁	Affinity (pK _i) ^a	Potency (pEC ₅₀) ^b	Efficacy (α) ^{b,c}
CXCL11	-	-	10.4 ± 0.0	9.2 ± 0.1	1.00 ± 0.01						
1	-	-	8.0 ± 0.1	- ^d	0.00 ± 0.01	30		H	6.4 ± 0.1	5.7 ± 0.3	0.42 ± 0.03
2a	-	-	7.4 ± 0.1	6.2 ± 0.1	0.96 ± 0.02	31		Cl	6.2 ± 0.1	- ^d	0.06 ± 0.01
5		H	6.3 ± 0.1	5.9 ± 0.2	0.20 ± 0.01	32		Cl	6.3 ± 0.1	- ^d	0.03 ± 0.02
6		H	7.0 ± 0.1	5.8 ± 0.1	0.73 ± 0.02	33		Cl	6.7 ± 0.1	6.1 ± 0.3	0.30 ± 0.03
23	H	H	5.6 ± 0.1	- ^d	0.04 ± 0.01	34		H	6.8 ± 0.1	5.9 ± 0.3	0.20 ± 0.02
24	Cl	H	6.7 ± 0.1	- ^d	0.02 ± 0.01	35		H	6.0 ± 0.1	5.1 ± 0.2	0.19 ± 0.02
25		H	6.2 ± 0.1	- ^d	0.11 ± 0.01	36		H	5.7 ± 0.1	- ^d	0.07 ± 0.01
26 ^e			6.4 ± 0.1	- ^d	0.03 ± 0.01	37		H	6.8 ± 0.0	4.9 ± 0.1	0.36 ± 0.02
27		H	6.6 ± 0.1	- ^d	0.05 ± 0.01	38		H	7.2 ± 0.1	6.1 ± 0.1	0.95 ± 0.03
28		H	6.4 ± 0.1	6.2 ± 0.1	0.31 ± 0.01	39		H	7.2 ± 0.0	6.0 ± 0.1	0.99 ± 0.02
29		H	6.6 ± 0.1	5.3 ± 0.1	0.64 ± 0.03	40		H	6.7 ± 0.0	- ^d	0.08 ± 0.02

^aMeasured by [¹²⁵I]CXCL10 displacement binding experiments with membranes prepared from HEK293 cells stably expressing the CXCR3 receptor. ^bMeasured by using a [³⁵S]GTPγS functional assay with membranes prepared from HEK293 cells stably expressing the CXCR3 receptor. ^cα represents the relative efficacy of a ligand compared to the endogenous agonist CXCL11 (which is set at α = 1.0). ^dCould not be determined due to the too low functional assay window. ^eThe point of attachment is colored red. All values shown are the mean ± SEM of at least three independent experiments.

outer ring as well. Subsequent SAR/SFR studies focused on the *ortho*-position of the outer ring and aimed to introduce groups differing in electronic properties and size. Introduction of one (34) or two (35) methyl groups resulted in weak partial agonism (α ≈ 0.2). An *o*-OH group (36) induced no significant functional agonism, and the affinity for this compound was the lowest in this series (pK_i = 5.7) (Table 1). Moderate to weak partial agonism was observed with an *o*-OMe (37; α = 0.36) or *o*-F (5; α = 0.20) substituent. However, the introduction of bigger halogen atoms, such as *o*-Br (38) or *o*-I (39), resulted in CXCR3 agonists that are able to reach the same maximum level of receptor activation (α = 0.95 and 0.99, respectively) as the endogenous peptide ligand CXCL11 (Figure 2B). Both 38 and 39 were comparably effective in terms of potency and efficacy, matching those of peptidomimetic agonist 2a (VUF10661).¹³

In contrast, mere shifting of the Br atom in 38 to the *meta*-position (as in 40) led to a complete loss of agonism, as had also been observed in the couple 6 versus 27 (Figure 2C). In all, the bigger halogens at the *ortho*-position of the outer ring were clearly preferred to provide full functional agonists.

2.2.2. Exploration of the Bicycloaliphatic Group. A selected set of compounds was subsequently prepared to explore the “left-hand” bicycloaliphatic side of the molecule. We have previously reported on the preference of CXCR3 for certain polycycloaliphatic groups,²¹ and within this class of biaryl ligands, the myrtenyl seems an attractive group.¹⁷ Given the subtle changes in activation pattern encountered in the biaryl moiety, we aimed for subtle changes in the bicycloaliphatic side of the molecule as well. Toward this end, saturated *endo*-myrtenyl analogues (41, 42) as well as derivatives with either

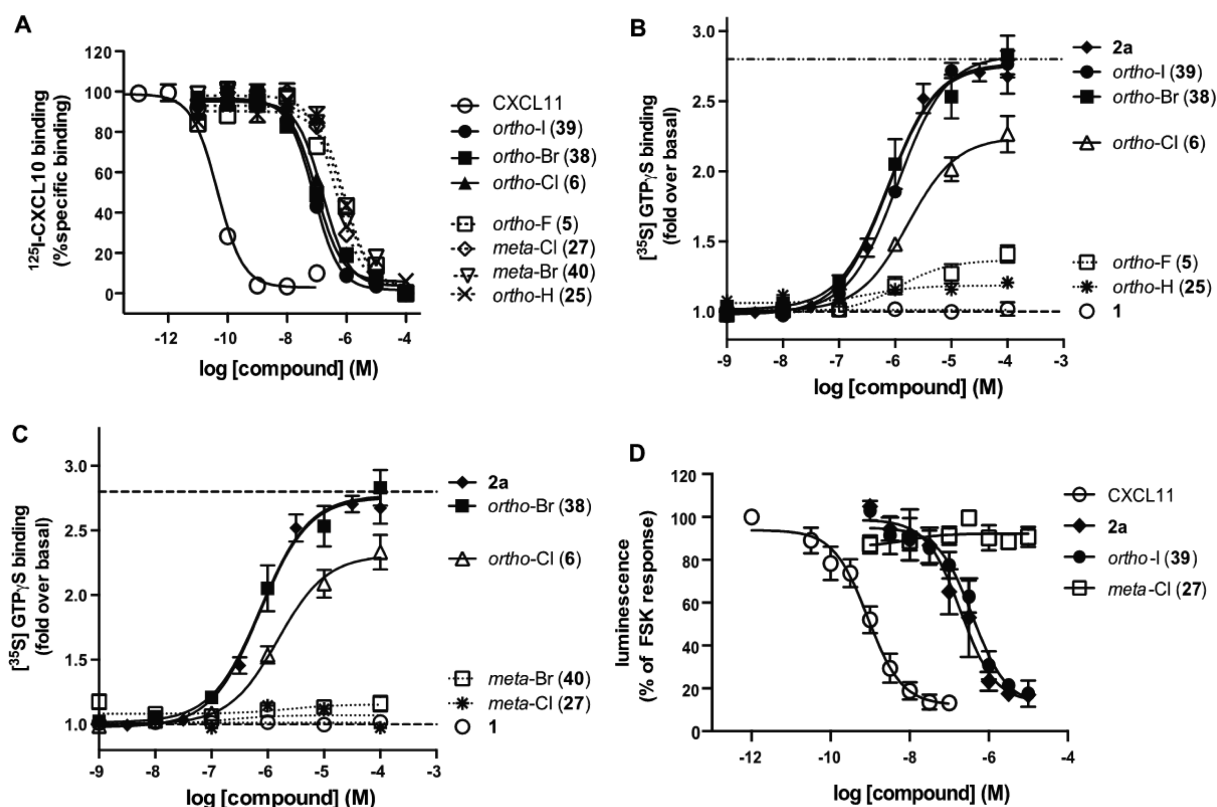


Figure 2. Radioligand binding curves and functional assay curves for selected compounds: (A) binding displacement assay using $[^{125}\text{I}]$ CXCL10 for key compounds, (B, C) $[^{35}\text{S}]$ GTP γ S functional assay for (B) compounds containing different (halogen) atoms on the *ortho*-position of the outer phenyl ring and for (C) compounds with a chloro or bromo group on the *ortho*- or *meta*-position of the outer phenyl ring, (D) CRE-luciferase reporter gene functional assay with key compounds on HEK293 cells transfected with the CXCR3 receptor and the CRE-luciferase reporter gene DNA. The graphs shown are the result of grouped data of at least three independent experiments. The dashed line (at 1.0) indicates basal levels of $[^{35}\text{S}]$ GTP γ S accumulation, whereas the dashed/dotted line (at 2.8) represents the maximal response (E_{max}) of the endogenous peptide agonist CXCL11 ($\alpha = 1$). Compounds 1 and 2a are included as a reference antagonist and agonist, respectively.

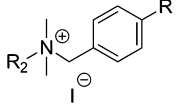
regioisomeric (43, 44) or stereoisomeric (45, 46) forms of the myrtenyl group were prepared (Table 2). A *m*-Cl or *o*-I moiety was kept as a “representative” biaryl portion of the antagonist and agonist subseries of this class, respectively. The results for 41–46 (Table 2) clearly show that the nature of the bicycloaliphatic group had only little effect on the affinity and, more importantly, on the functional profile of both the antagonist and the agonist subseries (compare 39 to 42/44/46 and 27 to 41/43/45). The most notable change observed was the small decrease in efficacy of 42 ($\alpha = 0.83$) compared to 39 ($\alpha = 0.99$) as a result of double bond reduction. The collective results not only suggest that these types of polycycloaliphatic architectures are indeed preferred anchors within this chemotype²¹ but also reinstate the biaryl portion as the major determinant for functional efficacy.

Functional effects on CXCR3 were inspected in more detail for key compounds 27 (no agonism) and 39 (full agonism). Activation of CXCR3 by 39 could be inhibited by addition of antagonist 1 and was absent in mock cells (Figure S1B,C, Supporting Information). We also used a CRE-luciferase reporter gene assay as an alternative to the $[^{35}\text{S}]$ GTP γ S functional assay. In this assay, 27 again did not show any agonism, whereas 39 showed full agonism comparable to peptidomimetic 2a (Figure 2D). All this unambiguously shows that the observed functional effect by 39 is elicited through specific interaction with the CXCR3 receptor. Collectively, our data on this nonpeptidomimetic class of ligands suggest a biaryl

o-halogen switch from antagonism to full agonism on CXCR3, which is not significantly influenced by subtle changes in the bicycloaliphatic moiety.

2.2.3. QM- and NOESY NMR-Based Studies. The SFR study reveals a link between the size and the location of the halogen substituent and the efficacy of the compound (e.g., 5, 6, 31, 38, and 39). As such, it is tempting to (partially) attribute this agonist switch to the change of the dihedral biaryl angle. To validate this hypothesis, QM calculations were performed to derive the optimal dihedral angle for each of the biaryl systems by performing a potential energy scan (key structures in Table 3, full listing in Table S1 and Figure S3, Supporting Information). Results from these simulations correspond to those from similar studies performed on biaryl systems.^{22,23} The angle of unsubstituted and *meta*-substituted compounds remains at ca. 40° (25, 27, 40). Due to steric hindrance, *ortho*,*ortho*-disubstituted compounds possess a typical dihedral angle of 90° (30, 33, 35), whereas the *ortho*-monosubstituted compounds possess a dihedral angle in the range of 45–70° depending on the size of the substituent (5, 6, 29, 34, 36, 38, 39). To correlate these QM-derived angles to experimentally determined angles, we resorted to quantitative NOESY NMR on selected compounds. Larger dihedral angles between the aromatic rings will result in a larger distance between the closest set of *ortho*-protons on adjacent rings (designated H' and H'', Table 4 and Figure S2A, Supporting Information). An indication for mean interatom distances can be obtained using

Table 2. Exploration of the Bicycloaliphatic Group



#	R	R ₂	Affinity (pK _i) ^a	Potency (pEC ₅₀) ^b	Efficacy (α) ^{b,c}
27			6.6 ± 0.0	- ^d	0.05 ± 0.01
39			7.2 ± 0.0	6.0 ± 0.1	0.99 ± 0.02
41			6.3 ± 0.1	- ^d	0.07 ± 0.01
42			7.0 ± 0.0	5.9 ± 0.1	0.83 ± 0.01
43			6.3 ± 0.0	- ^d	0.07 ± 0.01
44			6.7 ± 0.0	5.8 ± 0.1	1.05 ± 0.03
45			6.5 ± 0.0	- ^d	0.05 ± 0.01
46			7.3 ± 0.1	6.2 ± 0.1	0.98 ± 0.03

^aMeasured by [¹²⁵I]CXCL10 displacement binding experiments with membranes prepared from HEK293 cells stably expressing the CXCR3 receptor. ^bMeasured by a [³⁵S]GTPγS functional assay with membranes prepared from HEK293 cells stably expressing the CXCR3 receptor. ^cα represents the relative efficacy of a ligand compared to the endogenous agonist CXCL11 (which is set at α = 1.0). ^dCould not be determined due to the too low functional assay window for this low-efficacy compound. All values shown are the mean ± SEM of at least three independent experiments.

quantitative NOESY NMR through an r^{-6} dependence,^{24,25} and use of an absolute calibration distance elsewhere in the molecule allows reasonable approximation of unknown distances. For distance calibration we used the normalized sum of the H_a–H_c and H_b–H_c NOESY signals (¹H NMR shifts H_a and H_b overlap), since these are far away from the Y group and the rigidity of the myrtenyl group bodes well for using distances extracted from a crystal structure of an unrelated myrtenyl-containing compound.²⁶ The NOESY signal between the *ortho*-protons is a sum of the H'–H'' and H'–H''' NOESY effects, but at angles substantially smaller than 90° the r^{-6} dependence predicts that the measured signal can be attributed almost exclusively to the NOESY signal between the closest set of *ortho*-protons H' and H''. Indeed, our calculations (Table 4) suggest that the deviation in the experimentally determined H'–H'' distance as a result of interference of the more distant H'–H''' pair does not exceed 3.5% for the set of selected compounds, meaning that the NOESY measurements are

considered a reasonable approach for approximating the mean calculated angles. The distance H_d–H_e was measured as a control, as we expected Y not to have a significant influence on this distance. Selected *ortho*-substituted compounds with varying efficacies were subjected to NOESY NMR in CDCl₃ (5, 6, 25, 29, 34, and 38). Severe overlap of ¹H NMR signals in the aromatic region prohibited the inspection of key compound 39. A representative assignment and integration with compound 38 is shown in the Supporting Information (Figure S10). The results (Table 4) confirm that the reference H_d–H_e distance does not change with varying Y, while the H'–H'' distance depends on the size of the Y group: the larger Y groups induce a larger distance and hence a larger angle. The correlation between calculated and experimental data (Figure S2B) is good with minor deviations for the larger angles (interference of H'–H''', *vide supra*). This indicative correlation between theory and experiment shows that the calculated angles are representative of the actual dihedral angles under the measurement conditions and strengthens the confidence in the quantum mechanics calculations for the biaryl compounds.

With the confirmed calculated angles at hand, it is evident that, on average, ligands with a considerable efficacy (α > 0.5) seem to require a dihedral angle of around 60° (Figure 3). However, from the experimental results it is clear that the angle cannot be the sole determinant for agonism (e.g., compare 6 vs 31 or 6 vs 34). More particularly, the biaryl *ortho*-switch most likely has dual contributions from the spatial arrangement as well as from the electronic properties of the biaryl moiety. The possibility of a halogen bond, known to be especially applicable to the bigger halogens, also emerges in these considerations.^{27,28} As such, the electrostatic potential surfaces were calculated for the biaryl portion of the compounds (key structures in Table 3, full listing in Table S1, Supporting Information) as well as the electrostatic potential of the *ortho*-substituent. On the inner aryl ring, the electronegativity of the *ortho*-substituent influences the electrostatic potential close to the halogen (top views of 25 vs 27 and 38 vs 40) due to the proximity of the halogen p-orbital and the inner aryl ring at the optimal angle. On the outer aryl ring, the electrostatic potential (ESP) of the compounds depends on the amount of halogen atoms attached to the aryl ring. All compounds with only one halogen atom (5, 6, 27, 38, 39, and 40) possess an ESP of reciprocal magnitude (yellow surface), and all compounds with two halogen atoms (28, 29, and 30) possess an ESP of reciprocal magnitude (green surface). However, the value for the latter case (two halogen atoms) on the center of the aryl ring is more positive due to the electron-withdrawing properties of the additional halogen atom. Finally, the *o*-F group possesses a full negative hemisphere, whereas the heavier halogens introduce a positive potential (the so-called σ -hole²⁸) at the extension of the C–X axis (Table 3). With the increase of the halogen atom, the σ -hole becomes progressively stronger (5 < 6 < 38 < 39). Interestingly, this trend corresponds to the order of efficacies of these compounds (Table 3), suggesting another contributor to the agonism switch.

We compared the efficacy (α) with both the dihedral angle (φ, deg) of the optimal ligand conformation and the ESP (kcal/mol) at the van der Waals radius of the *o*-halogen (Figure 4A). A regression analysis, shown in Figure 4B, gave a significant correlation with α = 0.024(ESP) – 0.010φ + 0.979 (R = 0.89, R² = 0.79, R_{adj} = 0.71, SE = 0.17).

Table 3. Electron Density Surfaces Mapped with the Electrostatic Potential for Selected Compounds

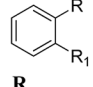


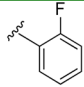
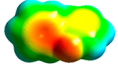
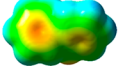
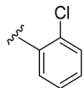
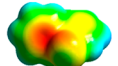
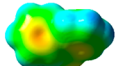
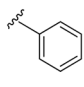
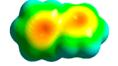
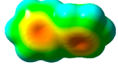
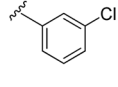
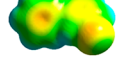
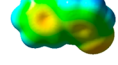
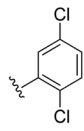
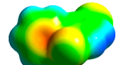
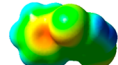
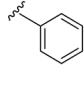
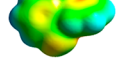
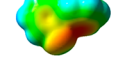
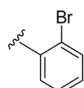
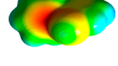
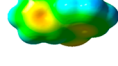
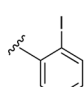
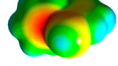
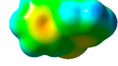
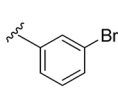
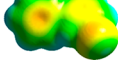
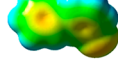
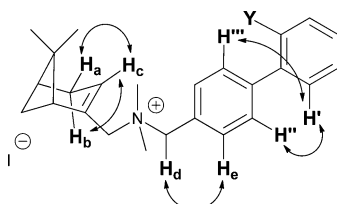
Related to		R	R ₁	Top view ESP -18.8 to 18.8 kcal/mol 	Bottom view ESP -18.8 to 18.8 kcal/mol 	Optimal Angle (°)	Efficacy (α)
5		F	H			43	0.20
6		Cl	H			58	0.73
25		H	H			40	0.11
27		Cl	H			39	0.05
29		Cl	H			58	0.64
31		Cl	Cl			58	0.06
38		Br	H			62	0.95
39		I	H			67	0.99
40		Br	H			40	0.08

Table 4. Experimental and Calculated Distances of Several Proton Pairs Based on QM Calculations and on Quantitative NOESY NMR Experiments^a

compd no.	Y	H ₁ -H _c (Å) (NOESY)	H'-H'' (Å) (NOESY)	H'-H'' (Å) (QM)	H'-H''' (Å) (QM)
5	F	2.34	2.37	2.40	4.41
6	Cl	2.32	2.58	2.68	4.16
25	H	2.33	2.40	2.40	4.42
29	2,5-di-Cl	2.33	2.66	2.69	4.16
34	Me	2.32	2.65	2.72	4.12
38	Br	2.33	2.63	2.76	4.09

^aThe graph depicts the hydrogen atom correlations used.

The results for the SFR, electrostatic potential surfaces and regression analysis collectively demonstrate that the *o*-halogen may be involved in halogen bonding and that this may play a role in the switch from antagonism to full agonism by possibly

stabilizing an active state of the CXCR3 receptor. The current case arguably illustrates the concept of “mechanism cliffs” (recently discussed²⁹) with subtle structural changes inducing switches in functional efficacies of small-molecule ligands.

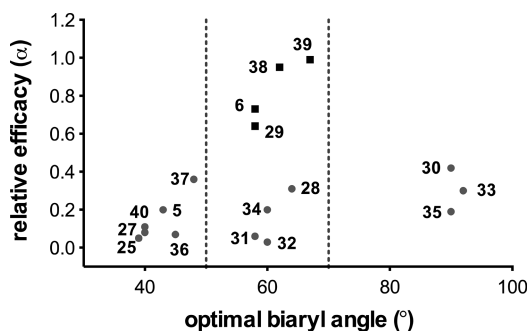


Figure 3. Ligands with considerable efficacy (greater than 0.5) have an angle of 60° on average. The calculated optimal angle between the two aryl rings is plotted against the efficacy measured in [³⁵S]GTPγS functional assays. The filled black squares highlight ligands that show an efficacy greater than 0.5, whereas the filled gray circles indicate ligands with an efficacy lower than 0.5. Data points are accompanied by the corresponding compound codes.

While this phenomenon appears to be more common for aminergic class A GPCRs,³⁰ mechanism cliffs for chemokine receptors are less frequently described.³¹ Notably, for CCR3 and for CCR5 a few subtle activation triggers have been disclosed.^{32–34} The structural class described in the present study includes a trigger that involves the mere size of a single atom (from F to Br and I) and can therefore be considered as displaying a very steep mechanism cliff for the chemokine CXCR3 receptor.

2.3. Conclusion. The molecular details of activation of peptide GPCRs by small molecules remain of both fundamental and practical relevance. Here, we describe the first reported nonpeptidomimetic agonists for the CXCR3 receptor. A total of 26 compounds, all possessing a bicycloaliphatic group and biaryl system linked through a quaternary ammonium cation, were prepared by versatile synthetic routes. A remarkably subtle trigger for receptor activation is present on the outer aryl ring of the biaryl system, and this allows for a full spectrum of functional efficacies to be achieved. Most notably, mere

enlargement of the halogen atom size on the *ortho*-position of the outer ring from F to Br (**38**) or I (**39**) furnishes full CXCR3 agonists, whereas moving the halogen group to the *meta*-position completely abolishes agonism. In contrast, modifications in the bicycloaliphatic group only had relatively minor effects on the agonist efficacies. QM and NOESY NMR were used to interrogate these phenomena. An important role is suggested for an optimal dihedral angle within the biaryl system of around 60°, and halogen bonding is hypothesized to be a key player in explaining the intriguing halogen effect. Collectively, we have described how an ensemble of chemical tools can be applied to explain a relevant chemical biology event. Practically, we present **38** (VUF11222) and **39** (VUF11418) as useful tools in CXCR3 research.

3. EXPERIMENTAL SECTION

3.1. Pharmacological Assays. **3.1.1. General Information.** All cell culture materials were purchased from PAA Laboratories GmbH (Pasching, Austria). [¹²⁵I]CXCL10 radioligand (2200 Ci/mmol) was obtained from Perkin-Elmer Life and Analytical Sciences (Boston, MA). Unlabeled CXCL11 was from Peprotech (Rocky Hill, NJ). All mentioned chemicals were purchased from Sigma-Aldrich (St. Louis, MO).

3.1.2. Cell Culture and Transfection. HEK293 cells stably expressing CXCR3 were a kind gift from Dr. K. Biber (University Medical Center, Groningen, The Netherlands) and were cultured as described previously.¹³ In the case of the CRE-luciferase reporter gene assay, the cells were transfected with plasmid containing the reporter gene CRE-luciferase as described in a previous report from our laboratory.³⁵

3.1.3. Membrane Preparation and Chemokine Binding Assay. Membrane preparation and competition radioligand bindings were performed as described previously¹³ with the exception that membranes from HEK293 cells stably expressing CXCR3 were used.

3.1.4. [³⁵S]GTPγS Functional Assay. The protocol used was as described previously.¹³ Briefly, 5 μg of membranes per well prepared from HEK293 cells stably expressing CXCR3 were incubated with CXCL11 or compounds in assay buffer containing 50 mM HEPES, 10 mM MgCl₂, and 100 mM NaCl, pH 7.2, supplemented with 3 μM GDP and 300 pM [³⁵S]GTPγS (Perkin-Elmer) for 1 h at room

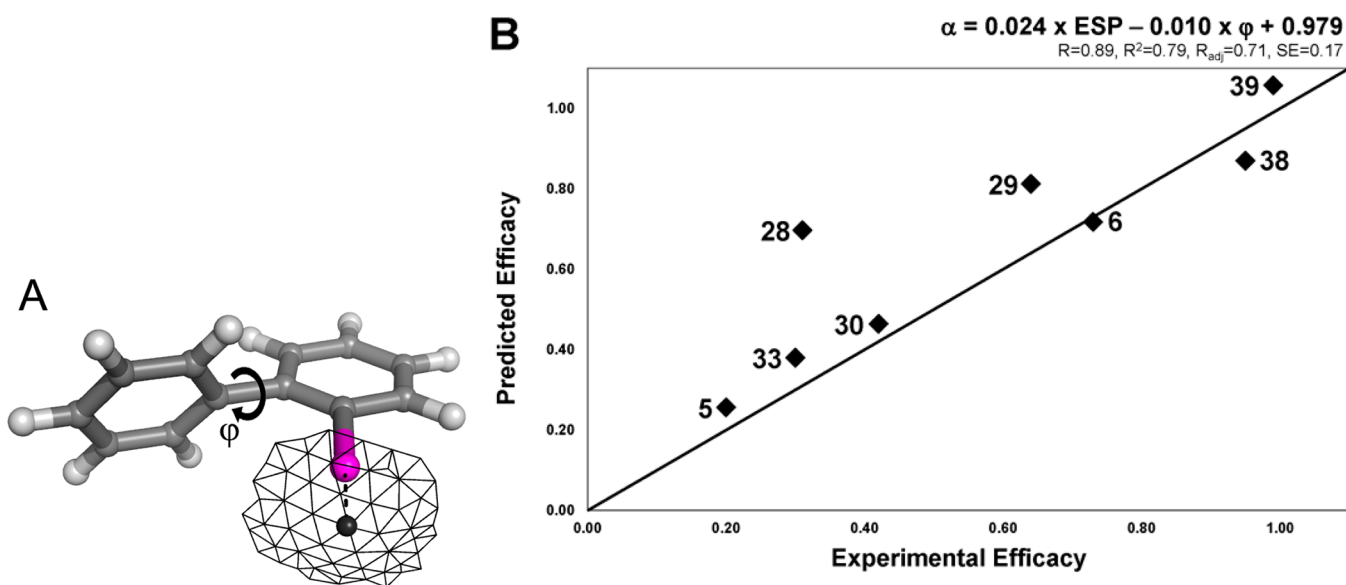


Figure 4. (A) Representation of the dihedral angle ϕ and the ESP at the extension of the C–X bond shown for **39**. (B) Predictive value of the regression analysis of the dihedral angle and the ESP to the experimental efficacy. Compound numbers are indicated for each individual data point in the figure.

temperature before harvesting of the membranes on Unifilter GF/B plates. [³⁵S]GTPγS incorporation was determined using the Microbeta. When the assay was run in antagonist mode, the compound was added 30 min prior to addition of [³⁵S]GTPγS. The response was normalized to that of the endogenous agonist CXCL11 (set to $\alpha = 1$). As such, this normalized response represents the relative efficacy of a given ligand presented as the α value.

3.1.5. CRE-Luciferase Reporter Gene Assay. This assay was performed as described previously.³⁵ In brief, culture medium was aspirated and replaced with serum-free medium supplemented with 0.05% BSA and ligands. After 5 h, stimulation medium was replaced by 25 μ L of substrate solution (39 mM Tris-H₃PO₄, pH 7.8, 39% glycerol, 2.6% Triton X-100, 860 μ M dithiothreitol, 18 mM MgCl₂, 825 μ M ATP, 77 μ M disodium pyrophosphate, 230 μ g/mL beetle luciferin), and luminescence was measured using a Victor³ plate reader (Perkin-Elmer).

3.1.6. Data Analysis. Nonlinear regression analysis of the data and calculation of pEC₅₀ and pK_i values were performed using Prism 5.0d (GraphPad Software Inc., San Diego, CA) as described before.¹³

3.2. Computational Methods. **3.2.1. Quantum Mechanical Calculations.** Quantum mechanical calculations were performed with Gaussian 03³⁶ using the Becke3LYP functional and the 6-311+G* basis set. For iodine, an additional SDD basis set was used. To alleviate computational complexity, only the biaryl portion was used, whereas the rest of the molecule was omitted from the calculations as this is not expected to influence the electron density distribution of the outer substituted phenyl ring. As such, for the remaining biaryl model system, different conformations were generated by performing a potential energy scan for the dihedral angle between the two phenyl rings. Due to ligand symmetry, calculations were performed for a dihedral angle between 0° and 180° with an interval of 30° (Figure S3, Supporting Information). Potential energy differences were calculated, and the lowest energy conformation was optimized with Gaussian to obtain the corresponding optimal dihedral angle. Subsequently, the ESP of the *ortho*-substituent was determined at the van der Waals radius of the halogen atom in the extension of the C-X bond. Distances between the *ortho*-hydrogen atoms of the phenyl rings for selected compounds were experimentally approximated by NOESY for the verification of our calculations (see the main text).

3.2.2. Data Regression. A 2D quantitative structure-activity relationship (QSAR) model was constructed using the ESP value and the dihedral angle of the optimized ligand conformations for a multiple linear regression to the efficacy. Data regression was performed using SPSS (SPSS Inc., Chicago, IL, 2005; <http://spss.com>).

3.3. Synthetic Methods. **3.3.1. General Information.** 2-Hydroxybenzeneboronic acid was from Alfa Aesar. All other chemicals were from Sigma-Aldrich. THF, toluene, and CH₂Cl₂ were distilled freshly from CaH₂; all other solvents were used as received. Compound **2a** was prepared as described by us.¹³ Unless indicated otherwise, all reactions were carried out under an inert atmosphere. TLC analyses were performed with Merck F254 alumina silica plates using UV visualization or staining. Microwave reactions were carried out on a Biotage initiator. Column purifications were carried out manually using Silicycle UltraPure silica gel or automatically using the Biotage equipment. All HRMS spectra were recorded on a Bruker micrOTOF mass spectrometer using ESI in positive ion mode. Elemental analysis was carried out at Mikroanalytisches Labor Pascher (Remagen, Germany). The ¹H, ¹³C, and 2D NMR spectra were recorded on a Bruker 200, 250, 400, or 500 MHz spectrometer. Infrared spectra were recorded on a Galaxy series FT-IR 6030 instrument. Systematic names for the molecules were generated using ChemBioDraw Ultra 11. Melting points were taken using the Stanford Research Systems Optimelt apparatus, and the values given are uncorrected. Optical rotations were measured with a sodium lamp and are reported as follows: [α]_D²⁵ (c, g/100 mL, solvent). Purities were measured with the aid of analytical LC-MS using a Shimadzu LC-20AD liquid chromatograph pump system with a Shimadzu SPD-M20A diode array detector with the MS detection performed with a Shimadzu LCMS-2010EV mass spectrometer. The column used was

an Xbridge (C18) 5 μ m column (50 mm \times 4.6 mm or 100 mm \times 4.6 mm). The four eluent programs used (acidic and basic) are listed in detail in the Supporting Information. Compound purities were calculated as the percentage peak area of the analyzed compound by UV detection at (unless mentioned otherwise) 230 nm. Unless reported otherwise, all compounds have a purity \geq 95% as measured by these LC-MS analyses.

3.3.2. General Procedure A1. A microwave vial was charged with the aryl bromide (0.90 mmol), the boronic acid (RB(OH)₂, 1.80 mmol), toluene (3 mL), *i*-PrOH (0.8 mL), and a 2.0 M Na₂CO₃ solution (0.50 mL). This mixture was degassed for 15 min by bubbling N₂ through the mixture using a needle. Next Pd(PPh₃)₄ (52 mg, 0.045 mmol) was added to the mixture, and the vial was immediately capped and again degassed for 5 min. The vial was heated in the microwave at 130 °C for (unless mentioned otherwise) 90 min. After this, the reaction mixture was filtered over Celite, and most of the organic solvents were evaporated in vacuo. The pH of the residue was adjusted to >11 with a 1.0 M aq NaOH solution, and the mixture was extracted with DCM (3 \times). The combined DCM layers were washed with brine, dried over Na₂SO₄, filtered, and concentrated in vacuo. This afforded the crude product, which was purified by column chromatography.

3.3.3. General Procedure A2. A microwave vial was charged with the aryl bromide (free base or salt, 1.0 mmol), the boronic acid (RB(OH)₂, 1.1 equiv), Na₂CO₃ (3.0 equiv in the case of aryl bromide salt, 2.0 equiv in the case of aryl bromide free base), DME (15 mL), and water (5 mL). This mixture was degassed for 15 min by bubbling N₂ through the mixture using a needle. Next Pd(PPh₃)₄ (0.05 equiv) was added to the mixture, and the vial was immediately capped and again degassed for 5 min. The vial was heated in the microwave at 120 °C for (unless mentioned otherwise) 60 min. After this, the reaction mixture was diluted with DCM and 2.0 M aq Na₂CO₃. Extraction was performed twice with DCM. The combined organic layers were dried over Na₂SO₄, filtered, and concentrated in vacuo. This afforded the crude product, which was purified by column chromatography.

3.3.4. General Procedure B. The amine (given amount) and aldehyde (1.0 equiv) were dissolved in DCE (given amount). The reaction mixture was stirred at rt for 30 min. Then NaBH(OAc)₃ (given amount) was added. After being stirred overnight (unless mentioned otherwise) at rt, the reaction was quenched with aq Na₂CO₃ (2.0 M). The mixture was stirred for 30 min at rt. The layers were separated, and the aqueous layer was extracted twice with DCM. The combined organic layers were dried over Na₂SO₄, filtered, and concentrated in vacuo to give the crude product, which was purified by column chromatography.

3.3.5. General Procedure C. In a round-bottom flask, the tertiary amine precursor (0.25 mmol) was dissolved in DCM (6.4 mL). The flask was placed under a nitrogen atmosphere, closed with a septum, and covered with aluminum foil. Then excess MeI (given amount) was added to the solution via a syringe. The reaction mixture was allowed to stir at rt in the dark. TLC analysis was used to monitor the progress of the reaction. If required, additional quantities of MeI were added followed by prolonged stirring. Such cycles were applied until completion of the reaction. The workup (unless mentioned otherwise) was as follows. The reaction mixture was cooled in an ice bath, and 3 vol equiv of MTBE was added to the reaction mixture slowly via a dropping funnel while the mixture was stirred. This usually caused precipitation of the salt. The precipitate was filtered and washed with a precooled solution of DCM/MTBE (1/3). Typically, this delivers the product salt in high purity. If required, the salt was either reprecipitated from DCM/MTBE as just described or recrystallized from hot DCM/MTBE. Occasionally (for example, in the case of **28** and **33**), in the initial precipitation with MTBE the salt does not precipitate as a solid but as a sticky oil. In those cases, the following procedure was used. The solution was concentrated in vacuo. A small amount of DCM was added, the mixture was gently warmed, and enough MTBE was added dropwise until slight turbidity appeared. Cooling to rt and then to -30 °C yielded a precipitate. This solid was filtered and washed with a precooled solution of DCM/MTBE (1/3). All final ammonium salts were thoroughly dried under high vacuum

and stored in the dark. Even then, some salts tended to retain DCM traces as crystal solvates, but these are considered noninterfering.

3.4. Representative Synthetic Examples. **3.4.1. 1-(2'-Bromobiphenyl-4-yl)-N-(((1*R*,5*S*)-6,6-dimethylbicyclo[3.1.1]hept-2-en-2-yl)methyl)-N-methylmethanamine (58).** A vial was charged with aldehyde **14** (150 mg, 0.57 mmol), amine **7** (95 mg, 0.58 mmol), NaBH(OAc)₃ (180 mg, 0.85 mmol), and DCE (3 mL) under a nitrogen atmosphere. The mixture was stirred for 16 h at rt. Then satd aq NaHCO₃ (3 mL) was added while the mixture was stirred. After 5 min, the mixture was diluted with DCM and water. Extraction was performed twice with DCM. The combined organic layers were dried over Na₂SO₄, filtered, and concentrated under vacuum. The crude product was purified by column chromatography (*n*-heptane/EtOAc/TEA, 100/0/1 to 80/20/1) to yield a colorless oil (115 mg, 49%). ¹H NMR (CDCl₃, 400 MHz): δ 7.66 (d, 1H, *J* = 7.9 Hz), 7.37–7.31 (m, 6H), 7.21–7.16 (m, 1H), 5.44 (br s, 1H), 3.59 (d, 1H, *J* = 13.4 Hz), 3.41 (d, 1H, *J* = 13.4 Hz), 2.97 (d, 1H, *J* = 13.2 Hz), 2.86 (d, 1H, *J* = 13.2 Hz), 2.47–2.41 (m, 1H), 2.36–2.21 (m, 3H), 2.17 (s, 3H), 2.15–2.09 (m, 1H), 1.31 (s, 3H), 1.18 (d, 1H, *J* = 8.6 Hz), 0.85 (s, 3H). ¹³C NMR (CDCl₃, 125 MHz): δ 146.4, 142.5, 139.5, 139.1, 133.1, 131.3, 129.2, 128.5, 127.3, 122.6, 119.7, 63.8, 61.3, 44.2, 42.6, 40.9, 37.9, 31.8, 31.4, 26.3, 21.1 (two aromatic carbon signals overlap). HR-MS (*m/z*): [M + H]⁺ for C₂₄H₂₉BrN, calcd 410.1483, found 410.1478 (doublet, peak at 412 also visible). LC purity: 99+%.

3.4.2. 1-(((1*R*,5*S*)-6,6-Dimethylbicyclo[3.1.1]hept-2-en-2-yl)-N-(2'-iodobiphenyl-4-yl)methyl)-N-methylmethanamine (59). A vial was charged with aldehyde **15** (75 mg, 0.24 mmol), amine **7** (40 mg, 0.24 mmol), NaBH(OAc)₃ (80 mg, 0.38 mmol), and DCE (5 mL) under a nitrogen atmosphere. The mixture was stirred for 16 h at rt. Then satd aq NaHCO₃ (3 mL) was added while the mixture was stirred. After 5 min, the mixture was diluted with DCM and water. Extraction was performed twice with DCM. The combined organic layers were dried over Na₂SO₄, filtered, and concentrated under vacuum. The crude product was purified by column chromatography (*n*-heptane/EtOAc/TEA, 100/0/1 to 80/20/1) to yield a colorless oil (85 mg, 77%). ¹H NMR (CDCl₃, 400 MHz): δ 7.92 (d, 1H, *J* = 8.1 Hz), 7.37–7.22 (m, 6H), 7.01–6.96 (m, 1H), 5.42 (br s, 1H), 3.56 (d, 1H, *J* = 13.3 Hz), 3.38 (d, 1H, *J* = 13.3 Hz), 2.94 (d, 1H, *J* = 13.1 Hz), 2.83 (d, 1H, *J* = 13.1 Hz), 2.44–2.37 (m, 1H), 2.33–2.18 (m, 3H), 2.15 (s, 3H), 2.12–2.06 (m, 1H), 1.28 (s, 3H), 1.16 (d, 1H, *J* = 8.6 Hz), 0.83 (s, 3H). ¹³C NMR (CDCl₃, 125 MHz): δ 146.6, 146.4, 142.6, 139.5, 139.1, 130.1, 129.0, 128.6, 128.5, 128.1, 119.8, 98.7, 63.8, 61.4, 44.2, 42.6, 40.9, 37.9, 31.8, 31.4, 26.3, 21.1. HR-MS (*m/z*): [M + H]⁺ for C₂₄H₂₉IN, calcd 458.1339, found 458.1329. LC purity: 98%.

3.4.3. 1-(2'-Bromobiphenyl-4-yl)-N-(((1*R*,5*S*)-6,6-dimethylbicyclo[3.1.1]hept-2-en-2-yl)methyl)-N,N-dimethylmethanaminium Iodide (38). The experimental procedure for this compound was performed according to the general methylation procedure (procedure C) using **58** (100 mg, 0.24 mmol) and MeI (300 μL, 4.82 mmol). The crude compound was reprecipitated according to the protocol described in procedure C. This afforded a white powder (125 mg, ca. 94%). Part of this product was recrystallized from warm MTBE/DCM. This gave a white solid (65 mg) which retained trace DCM solvate even after prolonged drying. This material was used for pharmacological studies. ¹H NMR (CDCl₃, 500 MHz): δ 7.73 (d, 2H, *J* = 8.2 Hz), 7.67 (dd, 1H, *J* = 8.0, 1.1 Hz), 7.49 (d, 2H, *J* = 8.2 Hz), 7.37 (app dt, 1H), 7.27 (dd, 1H, *J* = 7.6, 1.7 Hz), 7.23 (app dt, 1H), 6.28 (br s, 1H), 5.13 (s, 2H), 4.48 (d, 1H, *J* = 12.4 Hz), 4.32 (d, 1H, *J* = 12.4 Hz), 3.19 (s, 3H), 3.17 (s, 3H), 2.56–2.50 (m, 1H), 2.47–2.34 (m, 3H), 2.19–2.14 (m, 1H), 1.31 (s, 3H), 1.17 (d, 1H, *J* = 8.8 Hz), 0.87 (s, 3H). 2D NOESY NMR (CDCl₃, 500 MHz): see the Supporting Information. ¹³C NMR (CDCl₃, 125 MHz): δ 143.5, 141.0, 136.9, 136.1, 133.3, 133.0, 131.1, 130.3, 129.4, 127.6, 126.4, 122.2, 69.1, 66.8, 49.0, 48.8, 47.0, 39.7, 38.1, 32.1, 32.0, 25.9, 21.5. HR-MS (*m/z*): [M]⁺ for C₂₅H₃₁BrN, calcd 424.1634, found 424.1629 (doublet, peak at 426 also visible). LC purity: 99+%. The Supporting Information contains hardcopies of selected analytical data for **38**.

3.4.4. 1-(((1*R*,5*S*)-6,6-Dimethylbicyclo[3.1.1]hept-2-en-2-yl)-N-(2'-iodobiphenyl-4-yl)methyl)-N,N-dimethylmethanaminium Iodide (39). The experimental procedure for this compound was performed

according to the general methylation procedure (procedure C) using **59** (85 mg, 0.19 mmol) and MeI (300 μL, 4.82 mmol). The crude product was recrystallized from warm MTBE/DCM (3/1). This gave a white solid (80 mg, 70%). Part of this was recrystallized from warm MTBE/DCM (2/1) to give a white solid (33 mg) which retained trace DCM solvate (2.5 mol %) even after prolonged drying. This material was used for pharmacological studies. ¹H NMR (CDCl₃, 500 MHz): δ 7.95 (dd, 1H, *J* = 8.0, 1.0 Hz), 7.74 (d, 2H, *J* = 8.2 Hz), 7.43–7.38 (m, 3H), 7.25 (dd, 1H, *J*₁ obscured, *J*₂ = 1.7 Hz), 7.07 (app dt, 1H), 6.29 (br s, 1H), 5.13 (s, 2H), 4.49 (d, 1H, *J* = 12.4 Hz), 4.34 (d, 1H, *J* = 12.4 Hz), 3.19 (s, 3H), 3.18 (s, 3H), 2.57–2.51 (m, 1H), 2.48–2.35 (m, 3H), 2.20–2.15 (m, 1H), 1.32 (s, 3H), 1.18 (d, 1H, *J* = 8.8 Hz), 0.88 (s, 3H). 2D NOESY NMR (CDCl₃, 500 MHz): see the Supporting Information. ¹³C NMR (CDCl₃, 125 MHz): δ 146.5, 145.0, 139.7, 136.9, 136.1, 132.9, 130.2, 129.8, 129.4, 128.3, 126.4, 98.1, 69.3, 66.9, 49.0, 48.8, 47.0, 39.6, 38.1, 32.2, 32.0, 25.9, 21.5. HR-MS (*m/z*): [M]⁺ for C₂₅H₃₁IN, calcd 472.1496, found 472.1480. LC purity: 99+%. The Supporting Information contains hardcopies of selected analytical data for **39**.

■ ASSOCIATED CONTENT

Supporting Information

Supporting data on CXCR3 activation by key compounds, on QM calculations, and on NOESY NMR studies, procedures for NOESY NMR studies, syntheses, chromatographic details, and characterization of all compounds, representative 1D, 2D, and high-temperature NMR spectra, and selected LC chromatograms. This material is available free of charge via the Internet at <http://pubs.acs.org>.

■ AUTHOR INFORMATION

Corresponding Author

*Phone: +31 20 59 87579. Fax: +31 20 598 76 10. E-mail: r.leurs@vu.nl.

Present Address

¹Drug Discovery Biology, Monash Institute of Pharmaceutical Sciences, 399 Royal Parade, Parkville, Victoria 3052, Australia.

Author Contributions

[§]These authors contributed equally to this work.

Notes

The authors declare no competing financial interest.

■ ABBREVIATIONS USED

α, efficacy; DCE, 1,2-dichloroethane; DME, dimethoxyethane; ESP, electrostatic potential; GPCR, G protein-coupled receptor; GTPγS, guanosine 5'-O-[γ-thio]triphosphate; NOESY, nuclear Overhauser effect spectroscopy; QM, quantum mechanics; rt, room temperature; SAR, structure–activity relationship; SFR, structure–function relationship

■ REFERENCES

- (1) Overington, J. P.; Al-Lazikani, B.; Hopkins, A. L. How many drug targets are there? *Nat. Rev. Drug Discovery* **2006**, *5*, 993–996.
- (2) Scholten, D.; Canals, M.; Maussang, D.; Roumen, L.; Smit, M.; Wijnmans, M.; de Graaf, C.; Vischer, H.; Leurs, R. Pharmacological modulation of chemokine receptor function. *Br. J. Pharmacol.* **2012**, *165*, 1617–1643.
- (3) Viola, A.; Luster, A. D. Chemokines and their receptors: drug targets in immunity and inflammation. *Annu. Rev. Pharmacol. Toxicol.* **2008**, *48*, 171–197.
- (4) Medina, J. C.; Johnson, M. G.; Collins, T. L. CXCR3 antagonists. *Annu. Rep. Med. Chem.* **2005**, *40*, 215–225.
- (5) Wijnmans, M.; Verzijl, D.; Leurs, R.; de Esch, I. J.; Smit, M. J. Towards small-molecule CXCR3 ligands with clinical potential. *ChemMedChem* **2008**, *3*, 861–872.

- (6) Wijtmans, M.; de Esch, I. J. P.; Leurs, R. In *Chemokine Receptors as Drug Targets*; Smit, M. J., Lira, S. A., Leurs, R., Eds.; Wiley-VCH: Weinheim, Germany, 2011; pp 301–315.
- (7) Heise, C. E.; Pahuja, A.; Hudson, S. C.; Mistry, M. S.; Putnam, A. L.; Gross, M. M.; Gottlieb, P. A.; Wade, W. S.; Kiankarimi, M.; Schwarz, D.; Crowe, P.; Zlotnik, A.; Alleva, D. G. Pharmacological characterization of CXC chemokine receptor 3 ligands and a small molecule antagonist. *J. Pharmacol. Exp. Ther.* **2005**, *313*, 1263–1271.
- (8) O'Boyle, G.; Fox, C. R.; Walden, H. R.; Willet, J. D.; Mavin, E. R.; Hine, D. W.; Palmer, J. M.; Barker, C. E.; Lamb, C. A.; Ali, S.; Kirby, J. A. Chemokine receptor CXCR3 agonist prevents human T-cell migration in a humanized model of arthritic inflammation. *Proc. Natl. Acad. Sci. U.S.A.* **2012**, *109*, 4598–4603.
- (9) Yates, C. C.; Krishna, P.; Whaley, D.; Bodnar, R.; Turner, T.; Wells, A. Lack of CXC chemokine receptor 3 signaling leads to hypertrophic and hypercellular scarring. *Am. J. Pathol.* **2010**, *176*, 1743–1755.
- (10) Stroke, I. L.; Cole, A. G.; Simhadri, S.; Brescia, M. R.; Desai, M.; Zhang, J. J.; Merritt, J. R.; Appell, K. C.; Henderson, I.; Webb, M. L. Identification of CXCR3 receptor agonists in combinatorial small-molecule libraries. *Biochem. Biophys. Res. Commun.* **2006**, *349*, 221–228.
- (11) Angheliescu, A. V.; DeLisle, R. K.; Lowrie, J. F.; Klon, A. E.; Xie, X.; Diller, D. J. Technique for generating three-dimensional alignments of multiple ligands from one-dimensional alignments. *J. Chem. Inf. Model.* **2008**, *48*, 1041–1054.
- (12) Nedjai, B.; Li, H.; Stroke, I. L.; Wise, E. L.; Webb, M. L.; Merritt, J. R.; Henderson, I.; Klon, A. E.; Cole, A. G.; Horuk, R.; Vaidehi, N.; Pease, J. E. Small molecule chemokine mimetics suggest a molecular basis for the observation that CXCL10 and CXCL11 are allosteric ligands of CXCR3. *Br. J. Pharmacol.* **2012**, *166*, 912–923.
- (13) Scholten, D.; Canals, M.; Wijtmans, M.; de Munnik, S.; Nguyen, P.; Verzijl, D.; de Esch, I.; Vischer, H.; Smit, M.; Leurs, R. Pharmacological characterisation of a small-molecule agonist for the chemokine receptor CXCR3. *Br. J. Pharmacol.* **2012**, *166*, 898–911.
- (14) Wu, B.; Chien, E. Y. T.; Mol, C. D.; Fenalti, G.; Liu, W.; Katritch, V.; Abagyan, R.; Brooun, A.; Wells, P.; Bi, F. C.; Hamel, D. J.; Kuhn, P.; Handel, T. M.; Cherezov, V.; Stevens, R. C. Structures of the CXCR4 chemokine GPCR with small-molecule and cyclic peptide antagonists. *Science* **2010**, *330*, 1066–1071.
- (15) Roumen, L.; Sanders, M. P. A.; Vrolijk, B.; De Esch, I. J. P.; De Vlieg, J.; Leurs, R.; Klomp, J. P. G.; Nabuurs, S. B.; De Graaf, C. In silico veritas: the pitfalls and challenges of predicting GPCR-ligand interactions. *Pharmaceuticals* **2011**, *4*, 1196–1215.
- (16) Kufareva, I.; Rueda, M.; Katritch, V.; Stevens, R. C.; Abagyan, R. Status of GPCR modeling and docking as reflected by community-wide GPCR Dock 2010 assessment. *Structure* **2011**, *19*, 1108–1126.
- (17) Wijtmans, M.; Verzijl, D.; Bergmans, S.; Lai, M.; Bosch, L.; Smit, M. J.; de Esch, I. J. Leurs, R. CXCR3 antagonists: quaternary ammonium salts equipped with biphenyl- and polycycloaliphatic anchors. *Bioorg. Med. Chem.* **2011**, *19*, 3384–3393.
- (18) Oyler, K. D.; Coughlin, F. J.; Bernhard, S. Controlling the helicity of 2,2'-bipyridyl ruthenium(II) and zinc(II) hemicage complexes. *J. Am. Chem. Soc.* **2007**, *129*, 210–217.
- (19) Brown, H. C.; Dhokte, U. P. Hydroboration. 90. Synthesis of 2-isobutyl- and 2-isopropylapopinenes. Rates and stoichiometry of the hydroboration of 2-organylpopinenes with borane–methyl sulfide and borane–tetrahydrofuran. *J. Org. Chem.* **1994**, *59*, 2025–2032.
- (20) Simoni, D.; Giannini, G.; Roberti, M.; Rondanin, R.; Baruchello, R.; Rossi, M.; Grisolia, G.; Invidiata, F. P.; Aiello, S.; Marino, S.; Cavallini, S.; Siniscalchi, A.; Gebbia, N.; Crosta, L.; Grimaudo, S.; Abbadessa, V.; Di Cristina, A.; Tolomeo, M. Studies on the apoptotic activity of natural and synthetic retinoids: discovery of a new class of synthetic terphenyls that potently support cell growth and inhibit apoptosis in neuronal and HL-60 cells. *J. Med. Chem.* **2005**, *48*, 4293–4299.
- (21) Wijtmans, M.; Verzijl, D.; van Dam, C. M.; Bosch, L.; Smit, M. J.; Leurs, R.; de Esch, I. J. Exploring a pocket for polycycloaliphatic groups in the CXCR3 receptor with the aid of a modular synthetic strategy. *Bioorg. Med. Chem. Lett.* **2009**, *19*, 2252–2257.
- (22) Grein, F. Twist angles and rotational energy barriers of biphenyl and substituted biphenyls. *J. Phys. Chem. A* **2002**, *106*, 3823–3827.
- (23) Karpfen, A.; Choi, C. H.; Kertesz, M. Single-bond torsional potentials in conjugated systems: a comparison of ab initio and density functional results. *J. Phys. Chem. A* **1997**, *101*, 7426–7433.
- (24) Lipsitz, R. S.; Tjandra, N. Residual dipolar couplings in NMR structure analysis. *Annu. Rev. Biophys. Biomol. Struct.* **2004**, *33*, 387–413.
- (25) Anet, F. A. L.; Bourn, A. J. R. Nuclear magnetic resonance spectral assignments from nuclear Overhauser effects. *J. Am. Chem. Soc.* **1965**, *87*, S250–S251.
- (26) Veyrat, M.; Maury, O.; Faverjon, F.; Over, D. E.; Ramasseul, R.; Marchon, J.-C.; Turowska-Tyrk, I.; Scheidt, W. R. Chirophorphyrins: an approach to asymmetric catalysts with stereocenters near the plane of the porphyrin ring. *Angew. Chem., Int. Ed. Engl.* **1994**, *33*, 220–223.
- (27) Hardegger, L. A.; Kuhn, B.; Spinnler, B.; Anselm, L.; Ecabert, R.; Stihle, M.; Gsell, B.; Thoma, R.; Diez, J.; Benz, J.; Plancher, J. M.; Hartmann, G.; Banner, D. W.; Haap, W.; Diederich, F. Systematic investigation of halogen bonding in protein-ligand interactions. *Angew. Chem., Int. Ed.* **2011**, *50*, 314–318.
- (28) Parisini, E.; Metrangolo, P.; Pilati, T.; Resnati, G.; Terraneo, G. Halogen bonding in halocarbon-protein complexes: a structural survey. *Chem. Soc. Rev.* **2011**, *40*, 2267–2278.
- (29) Stumpfe, D.; Bajorath, J. Exploring activity cliffs in medicinal chemistry. *J. Med. Chem.* **2012**, *55*, 2932–2942.
- (30) Iyer, P.; Stumpfe, D.; Bajorath, J. Molecular mechanism-based network-like similarity graphs reveal relationships between different types of receptor ligands and structural changes that determine agonistic, inverse-agonistic, and antagonistic effects. *J. Chem. Inf. Model.* **2011**, *51*, 1281–1286.
- (31) Wise, E.; Pease, J. E. Unravelling the mechanisms underpinning chemokine receptor activation and blockade by small molecules: a fine line between agonism and antagonism? *Biochem. Soc. Trans.* **2007**, *35*, 755–759.
- (32) Anderskewitz, R.; Bauer, R.; Bodenbach, G.; Gester, D.; Gramlich, B.; Morschhauser, G.; Birke, F. W. Pyrrolidinohydroquinazolines—a novel class of CCR3 modulators. *Bioorg. Med. Chem. Lett.* **2005**, *15*, 669–673.
- (33) Ting, P. C.; Umland, S. P.; Aslanian, R.; Cao, J.; Garlisi, C. G.; Huang, Y.; Jakway, J.; Liu, Z.; Shah, H.; Tian, F.; Wan, Y.; Shih, N. Y. The synthesis of substituted biperidine amide compounds as CCR3 ligands: antagonists versus agonists. *Bioorg. Med. Chem. Lett.* **2005**, *15*, 3020–3023.
- (34) Ferain, T.; Hoveyda, H.; Ooms, F.; Schols, D.; Bernard, J.; Fraser, G. Agonist-induced internalization of CC chemokine receptor 5 as a mechanism to inhibit HIV replication. *J. Pharmacol. Exp. Ther.* **2011**, *337*, 655–662.
- (35) Watts, A. O.; Scholten, D. J.; Heitman, L. H.; Vischer, H. F.; Leurs, R. Label-free impedance responses of endogenous and synthetic chemokine receptor CXCR3 agonists correlate with G_i-protein pathway activation. *Biochem. Biophys. Res. Commun.* **2012**, *419*, 412–418.
- (36) Frisch, M. J.; Trucks, G. W.; Schlegel, H. B.; Scuseria, G. E.; Robb, M. A.; Cheeseman, J. R.; Montgomery, J. A., Jr.; Vreven, T.; Kudin, K. N.; Burant, J. C.; Millam, J. M.; Iyengar, S. S.; Tomasi, J.; Barone, V.; Mennucci, B.; Cossi, M.; Scalmani, G.; Rega, N.; Petersson, G. A.; Nakatsuji, H.; Hada, M.; Ehara, M.; Toyota, K.; Fukuda, R.; Hasegawa, J.; Ishida, M.; Nakajima, T.; Honda, Y.; Kitao, O.; Nakai, H.; Klene, M.; Li, X.; Knox, J. E.; Hratchian, H. P.; Cross, J. B.; Bakken, V.; Adamo, C.; Jaramillo, J.; Gomperts, R.; Stratmann, R. E.; Yazyev, O.; Austin, A. J.; Cammi, R.; Pomelli, C.; Ochterski, J. W.; Ayala, P. Y.; Morokuma, K.; Voth, G. A.; Salvador, P.; Dannenberg, J. J.; Zakrzewski, V. G.; Dapprich, S.; Daniels, A. D.; Strain, M. C.; Farkas, O.; Malick, D. K.; Rabuck, A. D.; Raghavachari, K.; Foresman, J. B.; Ortiz, J. V.; Cui, Q.; Baboul, A. G.; Clifford, S.; Cioslowski, J.; Stefanov, B. B.; Liu, G.; Liashenko, A.; Piskorz, P.; Komaromi, I.; Martin, R. L.; Fox, D. J.; Keith, T.; Al-Laham, M. A.; Peng, C. Y.;

Nanayakkara, A.; Challacombe, M.; Gill, P. M. W.; Johnson, B.; Chen, W.; Wong, M. W.; Gonzalez, C.; Pople, J. A. *Gaussian 03*, revision C.02; Gaussian, Inc.: Wallingford, CT, 2004.